AGU PUBLICATIONS

JGR

Journal of Geophysical Research: Biogeosciences

RESEARCH ARTICLE

10.1002/2015JG003044

Marsh-atmosphere CO_2 exchange in a New England salt marsh

Inke Forbrich[1] **and Anne E. Giblin**[1]

[1]The Ecosystems Center, Marine Biological Laboratory, Woods Hole, Massachusetts, USA

Key Points:
- Broadband NDVI was used to model NEE flux reduction during tidal inundation
- CO_2 flux reduction small at high marsh site, likely larger at lower elevation
- Climatic drivers more important for GPP than mean sea level during study period

Correspondence to:
I. Forbrich,
iforbrich@mbl.edu

Citation:
Forbrich, I., and A. E. Giblin (2015), Marsh-atmosphere CO_2 exchange in a New England salt marsh, *J. Geophys. Res. Biogeosci.*, *120*, 1825–1838, doi:10.1002/2015JG003044.

Received 5 MAY 2015
Accepted 30 AUG 2015
Accepted article online 5 SEP 2015
Published online 29 SEP 2015

Abstract We studied marsh-atmosphere exchange of carbon dioxide in a high marsh dominated salt marsh during the months of May to October in 2012–2014. Tidal inundation at the site occurred only during biweekly spring tides, during which we observed a reduction in fluxes during day and night. We estimated net ecosystem exchange (NEE), gross primary production (GPP), and ecosystem respiration (R_{eco}) using a modified PLIRTLE model, which requires photosynthetically active radiation, temperature, and normalized difference vegetation index (NDVI) as control variables. NDVI decreased during inundation, when the marsh canopy was submerged. Two-time series of NDVI, including and excluding effects of tidal inundation, allowed us to quantify the flux reduction during inundation. The effect of the flux reduction was small (2–4%) at our site, but is likely higher for marshes at a lower elevation. From May to October, GPP averaged -863 g C m^{-2}, R_{eco} averaged 591 g C m^{-2}, and NEE averaged -291 g C m^{-2}. In 2012, which was an exceptionally warm year, we observed an early start of net carbon uptake but higher respiration than in 2013 and 2014 due to higher-air temperature in August. This resulted in the lowest NEE during the study period (-255.9 ± 6.9 g C m^{-2}). The highest seasonal net uptake (-336.5 ± 6.3 g C m^{-2}) was observed in 2013, which was linked to higher rainfall and temperature in July. Mean sea level was very similar during all 3 years which allowed us to isolate the importance of climatic factors.

1. Introduction

Intertidal marshes have long been recognized for their important roles in coastal storm and erosion protection, nutrient removal, providing a nursery habitat for fisheries, and carbon sequestration [*Costanza et al.*, 1997], but they are increasingly threatened by sea level rise and anthropogenic activities. Ultimately, the long-term stability of salt marshes depends on their ability to accrete material at least at the same rate as sea level rises [*Morris et al.*, 2002]. Marsh vegetation plays a crucial role enhancing this capability. Shoots trap sediment that is suspended in flood water, an effect that increases with higher vegetation biomass [*Leonard and Luther*, 1995; *Mudd et al.*, 2010]. Furthermore, root growth contributes to soil organic matter accumulation [*Nyman et al.*, 2006; *Kirwan and Guntenspergen*, 2012]. Acknowledging these mechanisms has led to a renewed interest in understanding the controls on salt marsh production.

Field-based estimates of productivity have shown strong spatial gradients in productivity, shoot density, and standing stock of roots and rhizomes [*Valiela et al.*, 1978]. Studies on *Spartina alterniflora*, the dominant grass in the low marsh, have shown that soil salinity, dissolved sulfide, nitrogen availability, and elevation relative to sea level are local factors strongly influencing production and biomass [*Mendelssohn and Morris*, 2000; *Morris et al.*, 2002, 2013]. Less is known about the factors controlling local variation in the production of the marsh hay, *Spartina patens*, which is found on the high marsh [*Morris et al.*, 2013]. In general, measurements of the production of both species are complicated by the high spatial variability and by very high rates of below ground production, which is difficult to quantify reliably [*Valiela et al.*, 1976]. A different approach involves studying the ecosystem processes of photosynthesis and respiration and their environmental drivers. Micrometeorological flux methods like the eddy covariance technique [*Baldocchi et al.*, 1988] have been used widely in terrestrial ecosystems to study whole ecosystem fluxes of carbon dioxide (CO_2) and to estimate gross primary production (GPP), net ecosystem exchange (NEE), and ecosystem respiration (R_{eco}). One advantage of the method lies in the direct measurement of NEE without disturbing the soil or vegetation. Thus, the balance between carbon dioxide released and taken up by the ecosystem is measured, and model approaches allow the partitioning into the component fluxes GPP and R_{eco} [*Reichstein et al.*, 2005; *Lasslop et al.*, 2010]. However, this method is just beginning to be used in tidal wetlands [*Kathilankal et al.*, 2008; *Baldocchi*, 2014], where tidal dynamics offer special challenges when trying to apply the eddy covariance technique [*Barr et al.*, 2010].

Tidal inundation is a characteristic feature of coastal ecosystems, but its short-term duration and periodicities so far have prevented the application of empirical process models of NEE, GPP, or R_{eco}. Most studies only report NEE [*Kathilankal et al.*, 2008; *Moffett et al.*, 2010; *Artigas et al.*, 2015; *Schäfer et al.*, 2014], though information about the component fluxes and their drivers is necessary to understand long-term carbon cycling in these systems. One promising approach to assess the tidal influence on CO_2 fluxes is to compare the observed flux to a modeled flux under "nonflooded" conditions [*Kathilankal et al.*, 2008]. This requires consideration of environmental drivers (light and temperature) and effects of inundation. Inundation affects gas exchange not only by slow diffusion in the water column but also by reducing the air-exposed leaf area index (LAI) of the vegetation resulting in a decrease of CO_2 exchange [*Schedlbauer et al.*, 2010; *Koebsch et al.*, 2013]. In seasonally flooded wetlands, the effect on LAI can be monitored by satellite data like Moderate Resolution Imaging Spectroradiometer [*Koebsch et al.*, 2013]. In tidal wetlands, these tools can be used to analyze carbon fluxes along a regional inundation gradient [*Yan et al.*, 2008, 2010], but spatial and temporal resolution are too coarse for an application at a single site. However, reflectance measurements at the actual site and in sufficient temporal resolution have been used to improve CO_2 flux modeling when biomass was removed [*Wohlfahrt et al.*, 2010].

In this study, we argue that the main difference between "flooded" and "nonflooded" conditions for instantaneous NEE measurements is the amount of biomass that is air exposed, while all other environmental conditions stay identical. We use a broadband vegetation index estimated with sufficient temporal resolution as a proxy for biomass, taking advantage of the fact that reflectance properties of (partially) submerged canopies decrease with inundation level [*Beget and Bella*, 2007; *Kearney et al.*, 2009] thus mimicking a temporary reduction in biomass. The objective of this paper is to estimate seasonal NEE and its component fluxes in a New England salt marsh from eddy covariance measurements and assess the influence of tidal inundation. We report data from three growing seasons of a macrotidal system dominated by high marsh.

2. Materials and Methods

2.1. Site Description

The Plum Island Ecosystems Long-Term Ecological Research (PIE LTER) site is a coupled watershed and estuary in northeastern Massachusetts (Figure 1). The site experiences semidiurnal tides and the mean tidal range in this estuary is approximately 2.5 m. The highest astronomical tides that flood the entire marsh occur twice monthly around noon and midnight at the site, and the nighttime tides tend to be higher than the daytime tides (Figure 2). Mean high water at the site is ~1.3 m (in North American Vertical Datum of 1988 (NAVD88)), which roughly indicates the boundary between high marsh and low marsh areas. Vegetation on the high marsh platform is composed of *Spartina patens* and *Distichlis spicata* with stunted *Spartina alterniflora* occurring in areas with limited drainage. Low marsh areas are predominantly inhabited by *Spartina alterniflora*. Ponds occur in high and low marsh. They can be incised by creeks and drained, but due to increased sedimentation in these areas, *Spartina alterniflora* quickly inhabits these areas [*Wilson et al.*, 2014].

The LTER deploys a tide gauge (Ott, RLS) at the southern end of Plum Island Sound (Figure 1).

2.2. Micrometeorological Measurements

Fluxes of carbon dioxide (CO_2) were measured using the eddy covariance technique during the period of May to October of 2012–2014. Wind velocity and sonic temperature were measured by a 3-D sonic anemometer (Campbell Scientific CSAT-3A) mounted 4.16 m aboveground. Sample air was drawn from the central point of the anemometer through a 60 cm long tube to an infrared gas analyzer (Campbell Scientific EC155). Pump flow rate was 7l/min. These measurements were recorded with a frequency of 10 Hz. Air temperature and relative humidity were monitored at the same height as the anemometer (Campbell Scientific HC2S3). A four-component net radiometer (Hukseflux NR01) was mounted 1.5 m aboveground of the high marsh. At the same height, two sensors (LI190SB) monitored incoming and reflected photosynthetically active radiation (PAR). In addition, a pressure transducer (Campbell Scientific CS456) recorded water table height at the high marsh. In 2013 and 2014, an identical setup of instruments recorded values for an adjacent low marsh area.

The micrometeorological station was installed in the center of the high marsh platform (latitude: 42.736°, longitude: −70.828°). According to a rule of thumb, the fetch is normally assumed to be at least 100 times the measurement height [*Businger*, 1988]. Given the tower height of 4.16 m, we defined our study area as salt marsh occurring in a circle around the tower with a radius of 630 m excluding contributions from the adjacent Plum Island Sound or Rowley River. We used a digital elevation model [*Millette et al.*, 2010] to further

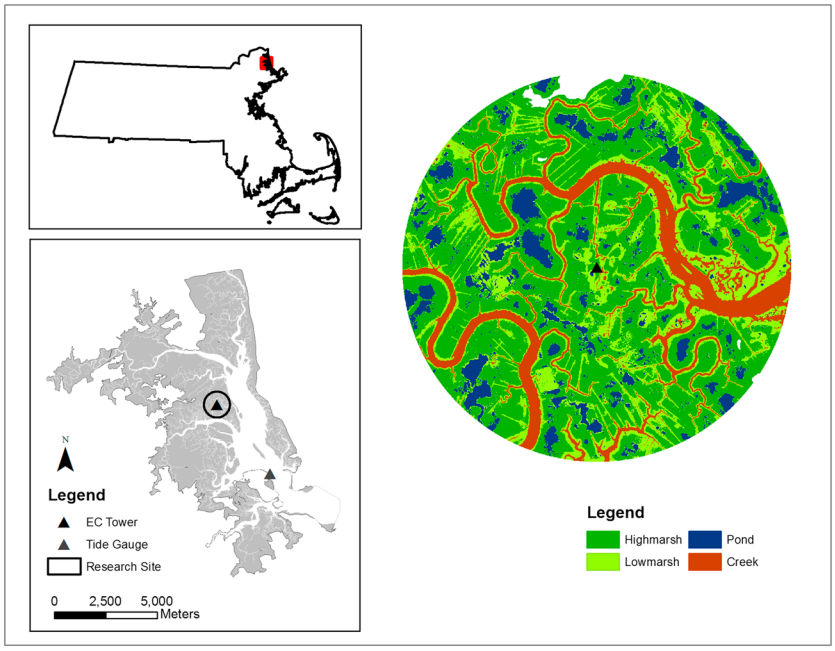

Figure 1. Overview of location: Inlet maps show location and boundaries of the PIE LTER estuarine research site as well as the location of study area and tide gauge within the estuary. Land cover characteristics of the study area were obtained from a digital elevation model [*Millette et al.*, 2010]. The site is a mosaic of marsh vegetation on high and low marsh, tidal creeks, and ponds. Coordinates of the tower location are 42.739°N, 70.828°W and radius is 630 m.

characterize the area. The area located at an elevation of below 0.6m NAVD88 was classified as tidal creeks. Low marsh was defined as ranging from 0.6 m to 1.3 m NAVD88. Above that threshold, high marsh occurred. The remaining area is characterized as permanent ponds, which we digitized from a 2011 aerial picture (2011 NOAA Ortho-rectified Mosaic of Merrimack River and Plum Island Sound, Massachusetts (Mean Lower Low Water)).

2.3. EC Flux Calculation and Quality Control

Since the EC155 records instantaneous CO_2 mixing ratios, fluxes were calculated directly from them [*Novick et al.*, 2013]. Two coordinate rotations were performed on the wind components, and the time lag between

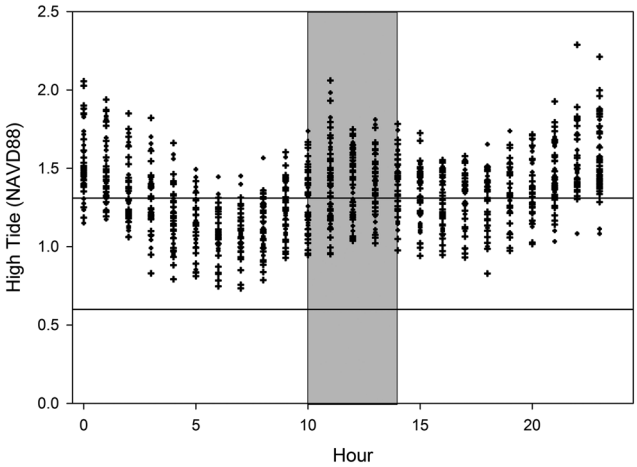

Figure 2. Timing and elevation of high tide of each tidal cycle within the investigation period. The horizontal lines indicate the lower elevation thresholds of low marsh at 0.6 m (NAVD88) and of high marsh at 1.31 m (NAVD88). Two high tides occur during the day which inundate the lower elevations more frequently than the high marsh. The shaded area indicates the time period around noon that we use to estimate normalized difference vegetation index (NDVI). Since the highest tides occur around noon, reflectance measurements at this time detect inundation.

wind and CO_2 mixing ratio measurements was determined and removed for each averaging interval of 30min. For every 30 min period, a factor for the correction of the frequency attenuation of the flux was calculated according to *Moore* [1986] and applied to the flux. Fluxes were calculated using the Edire software (version 1.5.0.32, R. Clement, University of Edinburgh, UK). Afterward, fluxes were filtered for system malfunctioning and calibration periods, integral turbulence characteristics, stationarity, and wind direction [*Foken et al.*, 2012]. We also excluded measurements when less than 75% of the flux was generated within the study area. This mostly occurred during stable nighttime conditions.

Thresholds in friction velocity (u_*) for nighttime fluxes were determined according to *Papale et al.* [2006]. It was set to 0.14 m/s for all three sampling seasons, respectively. On average, 41% of the observations were removed (66% of the nighttime fluxes and 21% of the daytime fluxes).

2.4. Spatial Analysis

2.4.1. Inundation Maps

To estimate the proportion of flooded versus nonflooded areas during each tidal cycle in the study area, we mapped the effect of different tide levels using a digital elevation model [*Millette et al.*, 2010] and available tide gauge data. We corrected the time series for a lag of 30 min which we observed between the tide level recorded at the mouth of the estuary (Figure 1) and the water table recorded on the high marsh at the tower. Thus, we created maps of flooded and nonflooded areas for each 30 min tide level during the study period. For flood maps, pixels with an elevation lower than the tide level were classified as 1 and areas with an elevation above it as 0. To estimate the proportion of land, the absence/presence code was reversed. Pond areas were excluded from the analysis based on elevation because they occurred in both low and high marsh [*Millette et al.*, 2010; *Wilson et al.*, 2014].

2.4.2. Source Area Estimation

To analyze the source area of the flux measurements, we used an analytical model according to *Kormann and Meixner* [2001]. We used six input variables: the effective aerodynamic measurement height, the horizontal wind speed at that height, the friction velocity, the roughness length (values were based on *Foken* [2008]), the Obhukov length, and the standard deviation of the crosswind.

To calculate the weighted fraction of the coverage of different land cover types within each 30 min source area, the output of the analytical model was combined with the flooding maps or the pond map. We constructed a coordinate system with the tower at the origin, and the respective image was rotated into the mean wind direction. For each map, the values of the two-dimensional source weight function were calculated for the central points of all pixels within the area of interest and were multiplied by their areas (1 m^2) and by the absence/ presence code of each map for all pixels in the area of interest. Their sum represents the fraction of the total source area (Ω). We scaled Ω so that their sum equals 100%.

2.5. NDVI Estimation and Processing

To continuously monitor the portion of the aboveground biomass that was not submerged, we calculated a broadband normalized difference vegetation index (NDVI) based on the approach of *Wilson and Meyers* [2007]. Incoming (i) and reflected (r) Solar (S) and photosynthetically active radiation (PAR) measurements were converted into red and near-infrared reflectance (ρ_{red} and ρ_{NIR}):

$$\rho_{red} = \frac{PAR_r}{PAR_i} \tag{1}$$

$$\rho_{NIR} = \frac{S_r - 0.45(S_i \rho_{red})}{0.55 S_i} \tag{2}$$

$$NDVI = \frac{\rho_{NIR} - \rho_{red}}{\rho_{NIR} + \rho_{red}} \tag{3}$$

Solar zenith effects were removed by using data exclusively around solar noon (10 A.M.–2 P.M. EST). Cloudy situations (S_i <300 W m^{-2}) and rainy periods were removed as well to ensure good quality reflectance data [*Wilson and Meyers*, 2007; *Rocha and Shaver*, 2009]. In our system, spring tides occurred around noon, so that simultaneous radiation measurements recorded the effect of tidal inundation at that time (Figure 2).

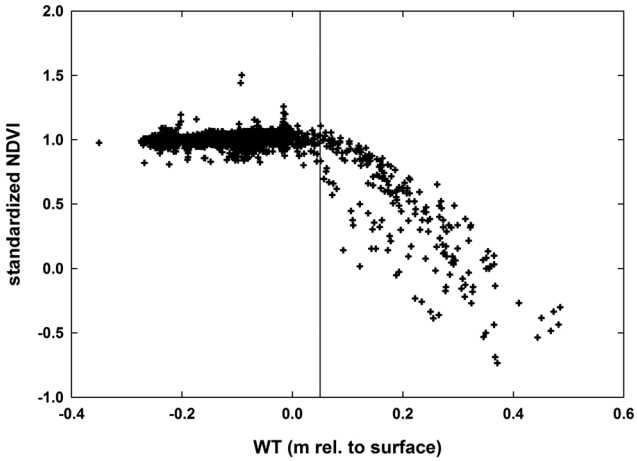

Figure 3. NDVI observations (10 min) from 2014 that are standardized to the maximum value plotted against the water table on the high marsh (1.31 m NAVD88). The line indicates the threshold above which NDVI decreases. A linear function is fitted to the data and used to interpolate flooding events during the night.

A decrease in NDVI would reflect that during inundation the amount of biomass that was air exposed was smaller than under nonflooded conditions.

We included this effect in our NEE model by creating two continuous time series of NDVI to simulate flooded and nonflooded conditions: $NDVI_{all}$ which included spring tide effects, and a reference time series, $NDVI_{ref}$, which represented nonflooded conditions. $NDVI_{ref}$ was calculated by creating daily averages from the noon estimates of NDVI not affected by inundation. This time series was smoothed and described a seasonal trend in biomass. To create a comparable time series including tidal effects ($NDVI_{all}$), we needed to isolate the tidal effects from the flooded NDVI data. We first standardized the noon time estimates using $NDVI_{ref}$ to remove seasonal trends. By plotting the standardized data against water table levels, we determined an empirical and likely site-specific threshold in water table level above which NDVI values decreased (Figure 3). A linear model was then fitted to the data that fell above this threshold. This fit was used to model NDVI values for each tidal cycle large enough to flood the marsh (WT > 0.05 m) using the continuous water table level data. Afterward, the standardization was removed, and modeled results were inserted into the time series of $NDVI_{ref}$ to create $NDVI_{all}$. Negative $NDVI_{all}$ values were set to 0.01 during fitting.

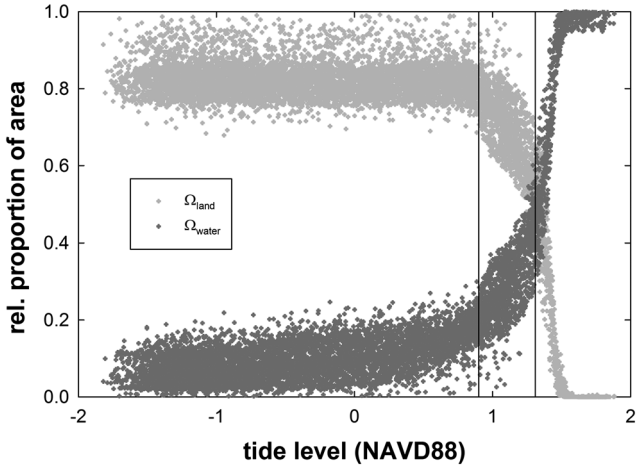

Figure 4. Source area fractions of marsh vegetation and water (Ω_{land} and Ω_{water}) along the tide height. Vertical lines indicate GPS values for low marsh and high marsh. At an elevation of 0.9 m NAVD88, Ω_{water} increased. With flooding of the high marsh areas at 1.31 m (NAVD88), the proportion of inundated areas in the flux source area quickly rise to 100%.

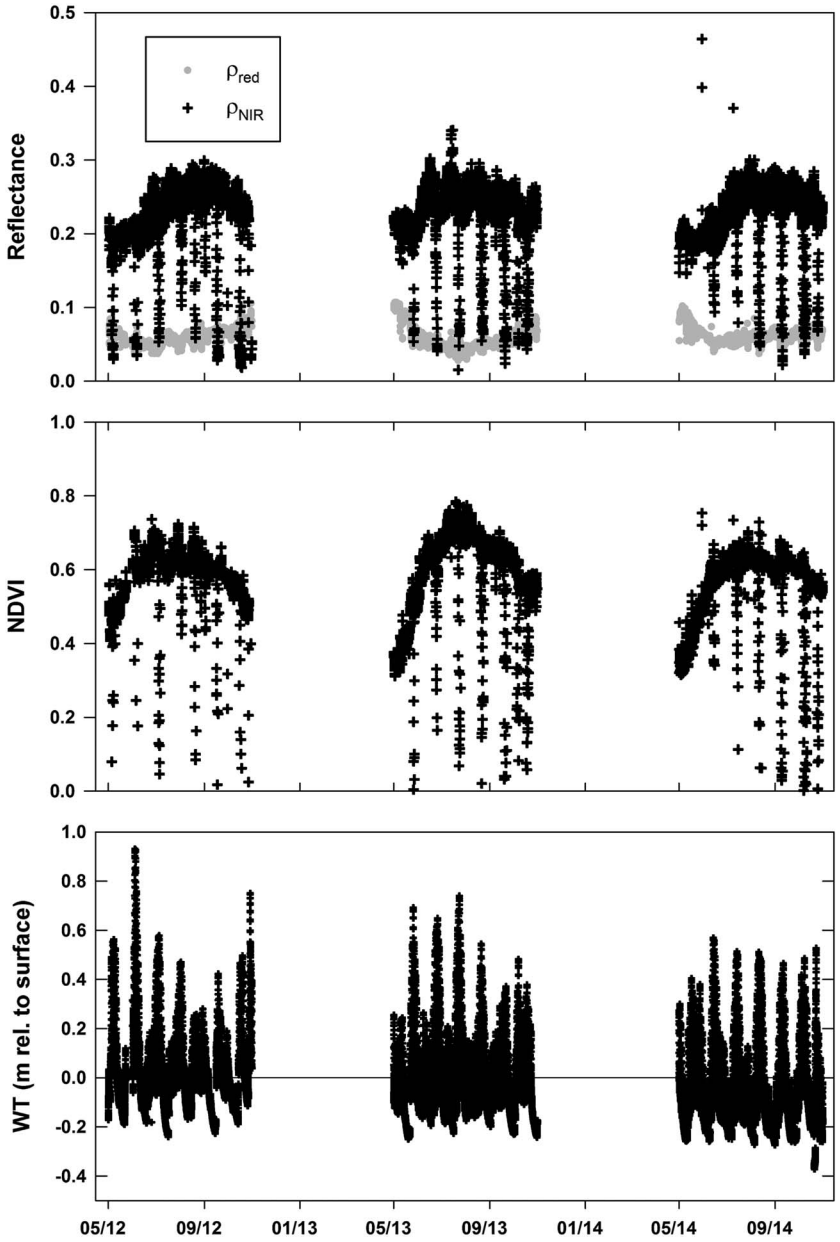

Figure 5. Seasonal and tidal variation in ρ_{red} and ρ_{NIR}, NDVI and water table. Seasonal variation in reflectance is characterized by a decrease in ρ_{red} and increase in ρ_{NIR} when the vegetation starts greening up. The short-term variation is due to a strong decrease in ρ_{NIR} when the canopy becomes submerged. This causes the NDVI to decrease during inundation. The water table on the high marsh shows that at this elevation, inundation occurs every second week with highest tides once a month. In the weeks between spring tides, the water table slowly drops below the surface.

2.6. Gap-Filling, Flux Partitioning, and Integrating Sums

To estimate daytime NEE, nonlinear light response curves like the common rectangular hyperbola are frequently used [*Falge et al.*, 2001]. These functions explain the functional relationship between daytime NEE and photosynthetic photon flux density (PPFD). Nighttime fluxes, which represent respiration, are modeled by a temperature dependent function like the Lloyd & Taylor model [*Reichstein et al.*, 2005], which can be combined with the light response curve [*Lasslop et al.*, 2010]. To model the effect of inundation on NEE, we introduced $NDVI_{all}$ as a third variable to estimate NEE. To model and partition the NEE fluxes, we modified the PLIRTLE model [*Shaver et al.*, 2007; *Rastetter et al.*, 2010], which requires LAI, air temperature, and PPFD as

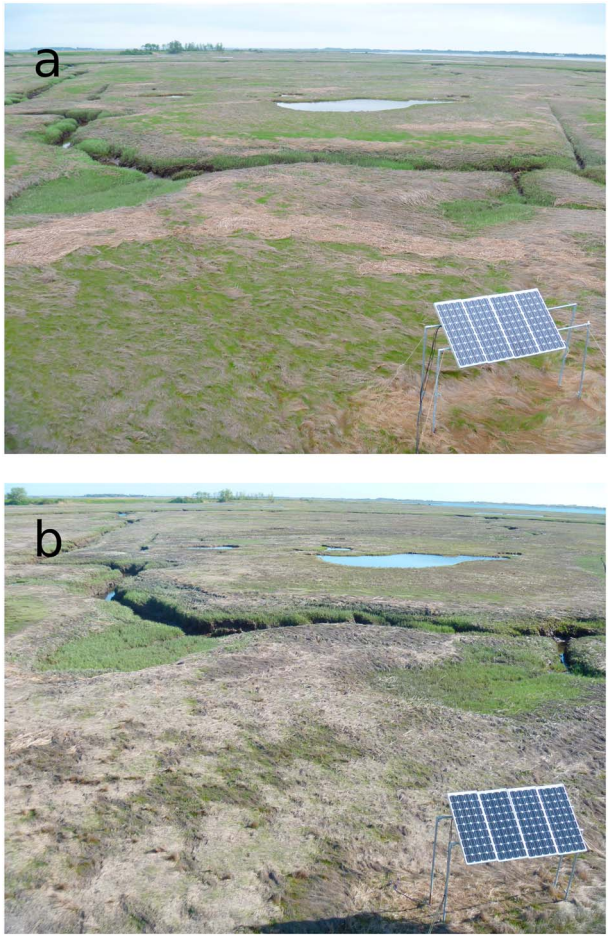

Figure 6. Photos taken from the flux tower looking north on 16 May 2012 and 2013. Marsh vegetation on high marsh is further developed in (a) 2012 than in (b) 2013.

controls. Instead of LAI, we used $NDVI_{all}$ and we adapted the Lloyd & Taylor model for the respiration term [*Reichstein et al.*, 2005]. By using the same parametrization with the time series of $NDVI_{ref}$ in a second run, we were able to estimate the effect of the flux reduction during inundation.

$$\mathrm{NEE} = \mathrm{GPP} + R_{\mathrm{eco}} \tag{4}$$

$$\mathrm{GPP} = \frac{P_{\max}}{k} * ln\left(\frac{P_{\max} + \alpha * I}{P_{\max} + \alpha * I * \exp{-k} * \mathrm{NDVI}}\right) \tag{5}$$

$$R = R_{\mathrm{ref}} * \mathrm{NDVI} * \exp\left(E_0 * \left(\frac{1}{T_{\mathrm{ref}} - T_0} - \frac{1}{T - T_0}\right)\right) \tag{6}$$

where NEE, GPP, and R_{eco} are net ecosystem exchange, gross primary production, and ecosystem respiration (all in µmol CO_2 m^{-2} s^{-1}). NDVI is the gap-filled time series of $NDVI_{all}$, I is the photosynthetic proton flux density (µmol m^{-2} s^{-1}), T is the air temperature (°C), T_{ref} is the reference temperature set to 10°C, and T_0 is −46.02°C [*Lloyd and Taylor*, 1994]. P_{max} is the light-saturated photosynthetic rate (µmolm^2 s^1), k is the Beer's light extinction coefficient (fixed to 0.5), and α is the initial slope of the light response curve (µmol CO_2 µmol photons^{-1}). R_{ref} is the temperature independent level of respiration (µmol CO_2 m^{-2} s^{-1}), while E_0 is a short-term temperature sensitivity parameter (µmol CO_2 m^{-2} s^{-1}) [*Reichstein et al.*, 2005].

E_0 for the respiration model was determined as short-term temperature sensitivity of R_{eco} and fixed for each season [*Reichstein et al.*, 2005]. Subsequently, P_{max}, E_0, and R_{ref} were estimated in a moving 4 day window for the central 2 days using both daytime and nighttime data [*Lasslop et al.*, 2010]. Parameter estimation was done using constrained least squares regression.

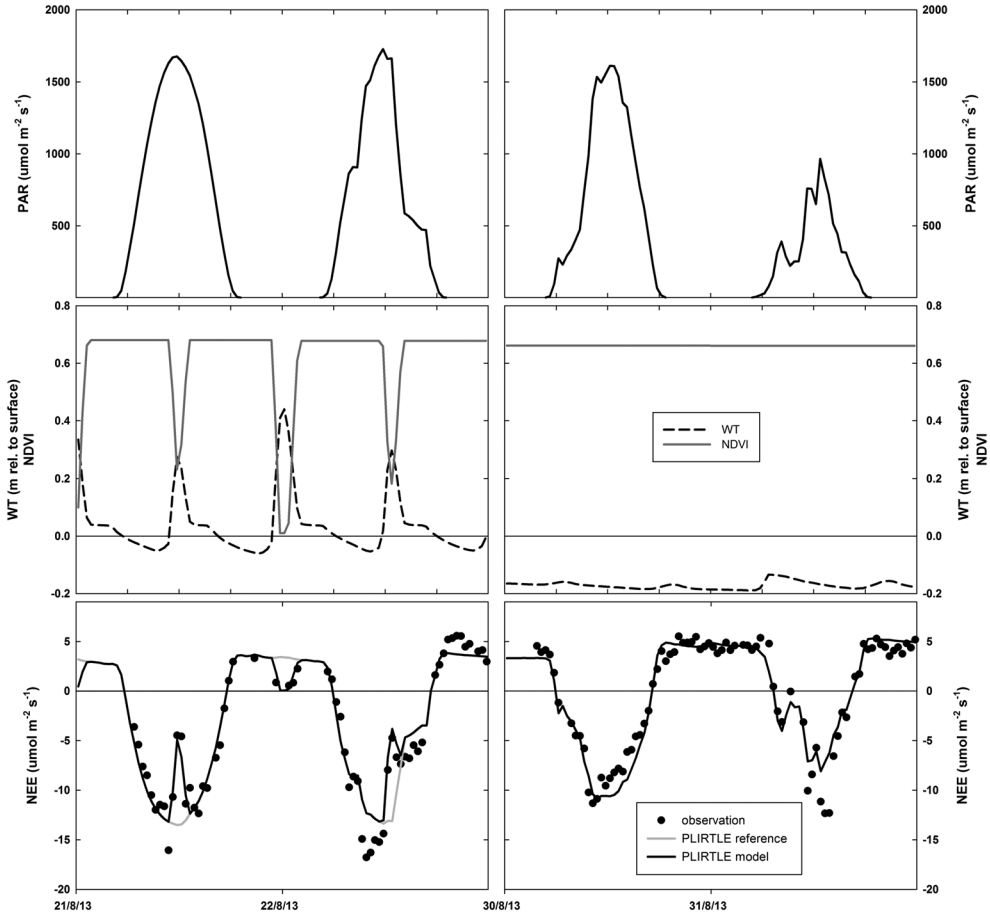

Figure 7. Example for different tidal stages and their effect on NEE: (top row) The photosynthetic active radiation indicating light conditions as well as day and night. (middle row) The water table relative to the high marsh surface and the corresponding NDVI. (bottom) NEE observations and PLIRTLE model fits. The black line indicates the model fit responding to inundation, the grey line indicates the reference flux under continuous air-exposed conditions.

The model based on inundation was also used for gap filling. We integrated the gap-filled time series over daily and seasonal time periods to estimate daily and seasonal sums. Similarly, we integrated the daily and seasonal component fluxes. We used a bootstrapping approach to estimate the model uncertainty [*Hagen et al.*, 2006]. We computed the integrated budget for each gap-filled bootstrapped data set, and we calculated the 95% confidence interval from the distribution of the 1000 bootstrapped budgets.

3. Results

3.1. Impact of Flooding on Source Area Composition

Over a tidal cycle, the proportion of vegetated marsh and water in the source area varied. When the tide level reached an elevation of 0.9 m (NAVD88), low marsh areas were submerged, but because most of the area was high marsh only about 20% was inundated (Figure 4). However, during spring tides at an elevation of 1.4m (NAVD88), the high marsh areas were also flooded leaving all vegetation submerged.

On average, 85% of the source area was marsh vegetation (56% high marsh and 29% low marsh), 9% creeks, and 6% permanent ponds.

3.2. Environmental Conditions

The mean temperature for the period of May–October in all 3 years was very similar with 17.6°C (2012), 17.3°C (2013), and 17.2°C (2014), but differences in seasons were observed. Spring temperatures (May) were highest in 2012, when average temperature (14.7°C) was 1° warmer and the minimum temperature (9.7°C) even 1.8 to 2.6° warmer than in the following years. Mean air temperatures in June (19.6°C) and July (23.3°C) were highest

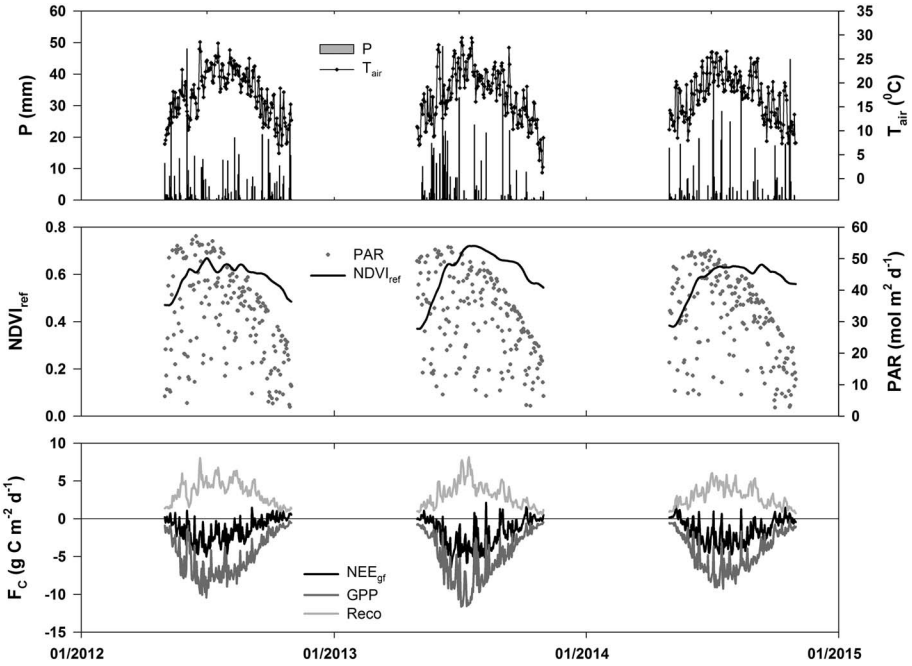

Figure 8. Seasonal dynamics of environmental variables and carbon dioxide fluxes: (top) Rainfall and air temperature from the PIE LTER meteorological station. (middle) The reference NDVI describing canopy development and PAR radiation. (bottom) The seasonality of NEE as well as of the component fluxes GPP and R_{eco}.

in 2013. Mean August temperatures (22.2°C) in 2012 again were 1.8–2.5 fold higher than in the following years, but fall temperatures (September and October) were similar again. Similarly, total rainfall during the observation months were in the same range for the 3 years (470 mm, 475 mm, and 484 mm), but the seasonal distribution was different. In 2012 and 2013, maximum rainfall occurred in July (2012: 125 mm and 2013: 177 mm), while in 2014 most rainfall was recorded in August (160 mm) and October (130 mm). Mean high water (May–October) in the 3 years did not vary much (1.32 m, 1.33 m, and 1.34 m in NAVD88).

3.3. Radiation Measurements and NDVI

Seasonal canopy development and tidal submergence led to a characteristic pattern in reflectance and NDVI (Figure 5). In spring, when the amount of live biomass increased, ρ_{red} decreased and ρ_{NIR} increased causing NDVI to increase. Throughout the growing season, NIR reflectance remained high while ρ_{red} showed some seasonal trend with an increase toward the end of the growing season, when *S. patens* turned brown. The NDVI remained high and only in 2012 got back to its spring level at the end of the measurement period. The date in spring when NDVI started increasing was very similar for the 3 years (Figure 5). However, the absolute values deviated between the years. On 16 May 2012, NDVI was higher (0.55) than in the other years (0.42), indicating an earlier growing season. This early greening was apparent on a larger scale than the radiation footprint (Figure 6).

Inundation caused ρ_{NIR} to decrease with no apparent change in ρ_{red}. Subsequently, the NDVI decreased and could become zero or negative during inundation, providing a very sensitive indicator of flooding of the vegetation.

3.4. Carbon Dioxide Fluxes

3.4.1. Inundation Effects

Tidal influences on NEE fluxes were observed both during the day and during the night, when the tide level was high enough to inundate the canopy of the high marsh vegetation. This was the case during spring tides that occurred around noon and midnight (Fig. 7). The effect was strongest during the summer months, when NEE fluxes were highest. While in spring, the NEE fluxes during inundation could turn positive during the day, later in the season the daytime NEE flux was smaller but remained negative.

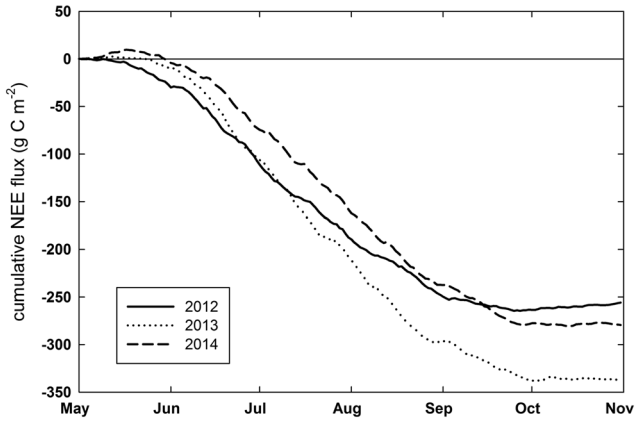

Figure 9. Seasonal cumulative NEE for the 3 years. A warm spring in 2012 caused an earlier net uptake of carbon dioxide than in the other two summers. In 2013 and 2014, spring dynamics are similar, but net uptake in summer 2013 is stronger than in both other years resulting in the largest seasonal uptake.

Even though parts of the source area flooded more frequently than the high marsh area, we did not observe strong suppression of NEE fluxes in those situations. Beside the smaller spatial coverage of the low marsh, the smaller impact was also due to variable timing of the flooding. Impact was minimal when high tides occurred early and late in the day, when NEE fluxes were already low. When high tide occurred during noon or midnight, the low marsh areas were inundated simultaneously with the spatially more dominant high marsh.

The modified PLIRTLE model described the dynamics of NEE very well during inundated and noninundated time periods, when used with a time series of $NDVI_{all}$ that responded to inundation. When used with a time series of $NDVI_{ref}$, the modified PLIRTLE model displayed the diurnal NEE dynamics entirely based on radiation and temperature resulting in larger fluxes than were actually observed during the inundation periods (Figure 7). The two modeled time series deviated only for periods of inundation. During these periods, differences in the 30min estimates could reach nearly 100%, especially for the nighttime fluxes.

3.4.2. Seasonality and Differences Between Years

Growing season dynamics of the system were well captured during May to October in each year. NEE values at the beginning of May and at the end of October were similarly low (Figure 8). During the summer months, GPP was generally larger than R_{eco} resulting in negative NEE during the entire season with exceptions during cloudy days. This was a similar dynamic as described by the NDVI, especially in 2013 when NDVI and CO_2 fluxes peaked in July. In the other years, NDVI values did not change much during the summer months. NEE during the summer months responded more strongly to changes in GPP than in R_{eco}.

While the seasonal trends in CO_2 fluxes were fairly similar in all 3 years (Figure 8), there were two periods when the flux deviated between the years. In May 2012, NEE values decreased earlier than in the other 2 years, due mostly to higher GPP. Years 2013 and 2014 showed a similar start of the growing season but deviated in the rest of the season which was mostly explained by the higher GPP during July (Figure 9).

3.4.3. Seasonal Budgets

Gap-filled NEE values for the period of 1 May to 31 October yielded -255.9 ± 6.9 g C m^2 (2012), -336.5 ± 6.3 g C m^2 (2013), and -279.5 ± 6.7 g C m^2 (2014) (Figure 9). Estimates for the component fluxes GPP and R_{eco} were derived with the model run that considered inundation and best fit the data. However, at our site, a comparison with estimates not including inundation showed that flux reductions were small (2–4%). GPP yielded -891.6 ± 11.5 g C m^2 (2012), -891.6 ± 8.8 g C m^2 (2013), and -806.1 ± 8.9 g C m^2 (2014). R_{eco} yielded 650.9 ± 13.5 g C m^2 (2012), 575.9 ± 12.6 g C m^2 (2013), and 545.7 ± 11.9 g C m^2 (2014).

4. Discussion

Eddy covariance measurements from similar sites along the U.S. Atlantic Coast are scarce, but our seasonal NEE values for the growing season compare reasonably with the annual value of -213 g C m^{-2} that were reported by *Artigas et al.* [2015] for a restored tidal salt marsh in New Jersey. *Schäfer et al.* [2014] report annual NEE values for another restoration site within that area, which are much more variable and range from carbon

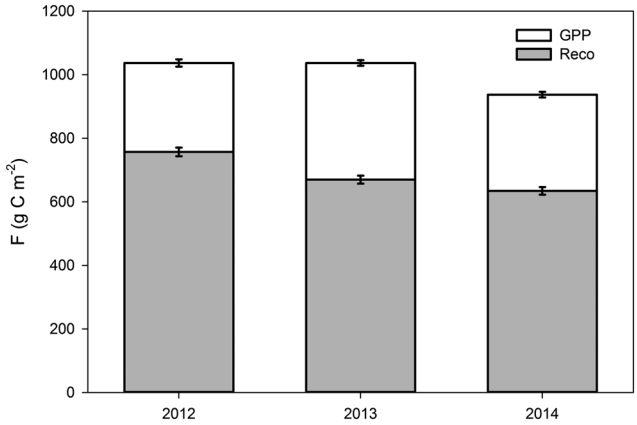

Figure 10. Seasonal budget estimates of GPP (converted to positive values) and R_{eco} that are scaled to 100% marsh vegetation. The error bars indicate the random uncertainty of the model estimate.

source to sink. This variability is linked to the management practices and not to climatic controls, however. At our site, we observed little interannual variability in CO_2 fluxes. Nevertheless, GPP was similar in 2012 and 2013 but smaller in 2014, which was supported by aboveground net primary productivity (NPP) estimates that showed a similar dynamic for these three seasons (J. Morris, unpublished data, 2015).

Marsh productivity (NPP) for Plum Island marshes and elsewhere has been linked to fluctuations in mean sea level or to rainfall during the peak growth month [*Morris and Haskin*, 1990; *Morris et al.*, 2013]. Both variables decrease the sediment salinity which increases at least aboveground growth. However, during our study period, the mean sea level did not vary much during the summer periods. Subsequently, pore water sulfide concentrations and salinity values taken monthly at long-term monitoring plots did not show any substantial variability between the three seasons (Morris, unpublished data). Even so, we did observe a peak in NDVI and CO_2 fluxes in July 2013 that corresponded to the highest rainfall in the growing season. Either we cannot resolve the effect of increased rainfall by only making monthly observations of pore water chemistry or salinity is not a major driver of productivity in that period.

Differences in GPP between 2013 and 2014 occurred in July when the temperature was different. Thus, temperature seems a more likely explanation for the observed variability in summer CO_2 fluxes. Spring temperatures in 2012 were above average in New England, causing earlier leaf out in forest ecosystems throughout the region [*Friedl et al.*, 2014]. In the marsh, we observed an earlier net uptake of carbon and highest spring GPP values in May 2012. Interestingly, though 2012 had a similar high GPP as 2013 but showed the lowest seasonal net uptake (Figure 9). Not only was the spring warm but also August temperatures were higher than in the other years, resulting in higher overall R_{eco} values (Figure 10).

We can detect tidal effects on marsh-atmosphere exchange only during flooding tides that are high enough to inundate the dominant high marsh. A suppression of fluxes occur during day and night, which supports findings by *Moffett et al.* [2010] and *Kathilankal et al.* [2008]. Sites studied by these authors are both dominated by marsh grass species which grow upright, either *Spartina alterniflora* [*Kathilankal et al.*, 2008] or *Spartina foliosa* and *Distichlis spicata* [*Moffett et al.*, 2010]. Water table thresholds indicating a decrease in fluxes at both sites are 17 cm and 25 cm. At our site, *Spartina patens* often lies prostrate forming a dense, green carpet with occasional "tussocks" or "cowlicks" [*Morris et al.*, 2013]. Our flooding threshold is much lower with 0.05 m above the surface. This indicates that not only tide range and elevation but vegetation height control the extent of flooding effects. However, in other tidal systems where the canopy grows tall, tidal effects on marsh-atmosphere exchange can look differently. This is most obvious for mangroves, where only a reduction in R_{eco} was observed because the canopy could not become submerged [*Barr et al.*, 2010]. Similarly, at a macrotidal site dominated by tall grasses (*Phragmites australis* and *Spartina alterniflora*), *Guo et al.* [2009] observe distinctive tidal fluctuations only for nighttime CO_2 fluxes. It seems possible that the canopy was not consistently submerged during the daytime tides. Under these conditions, a reduction in respiration during the day could arguably appear as an increase in carbon uptake during spring tides [*Guo et al.*, 2009; *Schäfer et al.*, 2014], contrasting with our results.

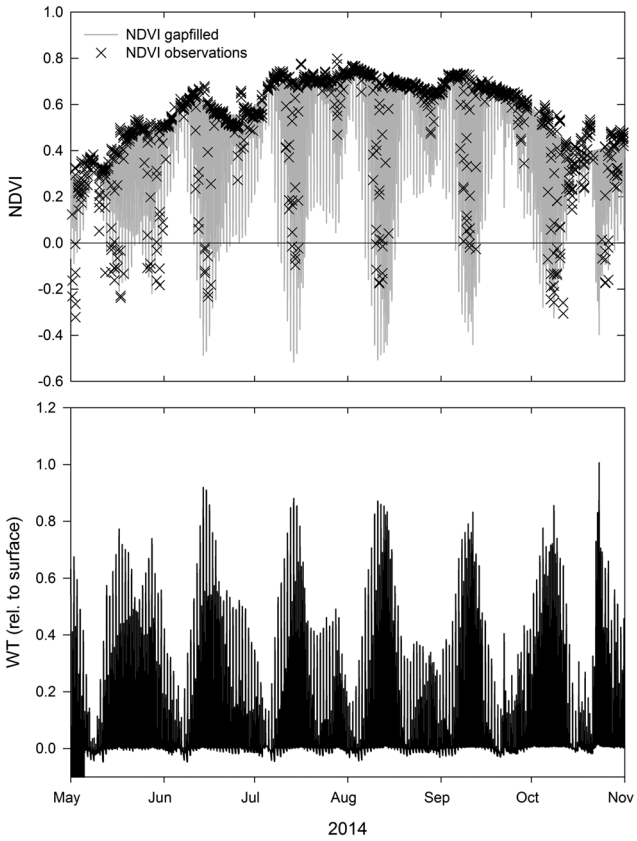

Figure 11. NDVI and water table level at a low marsh site (0.91 m NAVD88) indicate much more frequent flooding than on the high marsh (Figure 5).

At our site, flux reductions occur when the spatially dominant high marsh is submerged, which happens less frequently than at lower elevations. Similarly, *Artigas et al.* [2015] report for a restored marsh that water table level explained just 5% of variability in NEE fluxes measured above a mix of high and low marsh. However, we hypothesize that with more frequent flooding the effect of both GPP and R_{eco} will increase. Creating a synthetic data set based on our parametrization for NEE and the NDVI measurements from a low marsh in 2013 (Figure 11), we calculated the impact of flooding if the entire study area were low marsh. Under these conditions, differences in seasonal GPP and R_{eco} estimates due to flooding are about 10% and 14%, respectively, and thus much higher than the observed ones at our site of 2–4% (see above).

Several factors still need to be considered to fully understand inundation responses. Lab studies [*Wilson et al.*, 2014] as well as field measurements [*Kathilankal et al.*, 2011] have shown *Spartina* species capable of CO_2 uptake under water but at much reduced rates compared to air exposed leaves [*Wilson et al.*, 2014]. This would not be captured effectively by flux measurements between the surface and the atmosphere. Similarly, CO_2 release to the atmosphere is reduced during inundation, but concentrations of dissolved CO_2 concentrations in the surface water increase and are subjected to tidal export, which also is not captured with atmospheric flux measurements [*Troxler et al.*, 2015].

5. Conclusions

The tidal inundation of the marsh canopy at our site was monitored by using a broadband NDVI which decreased when the high marsh vegetation was inundated. Using a modified PLIRTLE model [*Shaver et al.*, 2007], which requires NDVI, radiation, and temperature as variables, allowed us to estimate NEE, GPP, and R_{eco} and model the flux reduction that we observed during inundation. Since we observed flux reduction only during biweekly spring tides that were high enough to inundate the high marsh canopy, the effect of inundation on seasonal integrated carbon fluxes in our system was small. This was likely due to the relatively high elevation of our site. We hypothesize a larger effect on carbon fluxes at lower elevation.

Table A1. Parameter Settings During Estimation Routine and Range of Observed Parameter Values

Parameter	Initial Guess	Constrains	Observed Range
E_0	100	50–400	205.2–221.7
P_{max}	3rd to 97th quantile of daytime NEE	3–0.2*initial guess	−75.7–2.8
α	−0.05	−0.01–1	−0.01–0.1
R_{ref}	1	0.5–10	1.3–5.6

Net carbon uptake in the 3 years studied started in May and decreased toward fall. Significant differences were observed in 2013 and 2014 as compared to 2012, when unusual warm temperatures caused an early green up and warm August temperature caused an increase in respiration. Years 2013 and 2014 were more typical in the seasonal pattern, with GPP peaks in July. Higher July temperatures and rainfall in 2013 resulted in higher GPP than in 2014. Interannual variability of marsh productivity at our site has been linked to variations in mean sea level. However, during our study period mean sea level did not vary much in all years, allowing us to observe the importance of climatic drivers on marsh productivity.

Appendix A: Model Parametrization

The fit parameters in our model showed considerable seasonality to account for ecological processes not included in the PLIRTLE model. Values for the light-saturated photosynthetic rate, the initial slope of the light response curve and the temperature independent level of respiration increase toward peak season (June to August) and decrease afterward. E_0 for the respiration model was determined as short-term temperature sensitivity of R_{eco} and fixed for each season [*Reichstein et al.*, 2005]. Subsequently, P_{max}, E_0, and R_{ref} were estimated in a moving 4 day window for the central 2 days using both daytime and nighttime data [*Lasslop et al.*, 2010]. Parameter estimation was done using constrained least squares regression. Table A1 contains information about the fitting procedure.

Acknowledgments
The data for this paper are available upon request from the authors and will be made available within the LTER database. We would like to thank Sam Kelsey, Sam Bond, Catherine Caruso, Colin Millar, and Jimmy Nelson (all MBL) for help during the installation and taking out of the equipment. Karen Sundberg (University of South Carolina) digitized pond. Chuck Hopkinson (UGA), Jim Morris (University of South Carolina), and Ed Rastetter (MBL) improved the study with helpful discussions. In addition, we would like to thank two anonymous reviewers for their suggestions and comments. Jane Tucker (MBL) proofread the manuscript. PIE LTER is funded by NSF grants OCE-1058747 and OCE-1238212.

References

Artigas, F., J. Y. Shin, C. Hobble, A. Marti-Donati, K. V. Schäfer, and I. Pechmann (2015), Long term carbon storage potential and CO_2 sink strength of a restored salt marsh in New Jersey, *Agric. For. Meteorol.*, *200*, 313–321.

Baldocchi, D. (2014), Measuring fluxes of trace gases and energy between ecosystems and the atmosphere—The state and future of the eddy covariance method, *Global Change Biol.*, *20*(12), 3600–3609.

Baldocchi, D. D., B. B. Hincks, and T. P. Meyers (1988), Measuring biosphere-atmosphere exchanges of biologically related gases with micrometeorological methods, *Ecology*, *69*(5), 1331–1340.

Barr, J. G., V. Engel, J. D. Fuentes, J. C. Zieman, T. L. O'Halloran, T. J. Smith, and G. H. Anderson (2010), Controls on mangrove forest-atmosphere carbon dioxide exchanges in Western Everglades National Park, *J. Geophys. Res.*, *115*, G02020, doi:10.1029/2009JG001186.

Beget, M., and C. D. Bella (2007), Flooding: The effect of water depth on the spectral response of grass canopies, *J. Hydrol.*, *335*(3-4), 285–294.

Businger, J. (1988), Evaluation of the accuracy with which dry deposition can be measured with current micrometeorological techniques, *J. Clim. Appl. Meteorol.*, *25*, 1100–1124.

Costanza, R., et al. (1997), The value of the world's ecosystem services and natural capital, *Nature*, *387*, 253–260.

Falge, E., et al. (2001), Gap filling strategies for defensible annual sums of net ecosystem exchange, *Agric. For. Meteorol.*, *107*(1), 43–69.

Foken, T. (2008), *Micrometeorology*, Springer, Berlin.

Foken, T., R. Leuning, S. R. Oncley, M. Mauder, and M. Aubinet (2012), Corrections and data quality control, in *Eddy Covariance - A Practical Guide to Measurement and Data Analysis*, edited by M. Aubinet, T. Vesala, and D. Papale, pp. 86–132, Springer, Netherlands.

Friedl, M. A., J. M. Gray, E. K. Melaas, A. D. Richardson, K. Hufkens, T. F. Keenan, A. Bailey, and J. O'Keefe (2014), A tale of two springs: Using recent climate anomalies to characterize the sensitivity of temperate forest phenology to climate change, *Environ. Res. Lett.*, *9*(5), 054006.

Guo, H., A. Noormets, B. Zhao, J. Chen, G. Sun, Y. Gu, B. Li, and J. Chen (2009), Tidal effects on net ecosystem exchange of carbon in an estuarine wetland, *Agric. For. Meteorol.*, *149*(11), 1820–1828.

Hagen, S. C., B. H. Braswell, E. Linder, S. Frolking, A. D. Richardson, and D. Y. Hollinger (2006), Statistical uncertainty of eddy flux-based estimates of gross ecosystem carbon exchange at Howland Forest, Maine, *J. Geophys. Res.*, *111*, D08S03, doi:10.1029/2005JD006154.

Kathilankal, J., T. Mozdzer, J. Fuentes, K. McGlathery, P. D'Odorico, and J. Zieman (2011), Physiological responses of Spartina alterniflora to varying environmental conditions in Virginia marshes, *Hydrobiologia*, *669*(1), 167–181.

Kathilankal, J. C., T. J. Mozdzer, J. D. Fuentes, P. D'Odorico, K. J. McGlathery, and J. C. Zieman (2008), Tidal influences on carbon assimilation by a salt marsh, *Environ. Res. Lett.*, *3*(4), 044010.

Kearney, M. S., D. Stutzer, K. Turpie, and J. C. Stevenson (2009), The effects of tidal inundation on the reflectance characteristics of coastal marsh vegetation, *J. Coastal Res.*, *256*, 1177–1186.

Kirwan, M. L., and G. R. Guntenspergen (2012), Feedbacks between inundation, root production, and shoot growth in a rapidly submerging brackish marsh, *J. Ecol.*, *100*(3), 764–770.

Koebsch, F., S. Glatzel, J. Hofmann, I. Forbrich, and G. Jurasinski (2013), CO_2 exchange of a temperate fen during the conversion from moderately rewetting to flooding, *J. Geophys. Res. Biogeosci.*, *118*, 940–950, doi:10.1002/jgrg.20069.

Kormann, R., and F. Meixner (2001), An analytical footprint model for non-neutral stratification, *Boundary Layer Meteorol.*, *99*(2), 207–224.

Lasslop, G., M. Reichstein, D. Papale, A. D. Richardson, A. Arneth, A. Barr, P. Stoy, and G. Wohlfahrt (2010), Separation of net ecosystem exchange into assimilation and respiration using a light response curve approach: Critical issues and global evaluation, *Global Change Biol.*, *16*(1), 187–208.

Leonard, L. A., and M. E. Luther (1995), Flow hydrodynamics in tidal marsh canopies, *Limnol. Oceanogr.*, *40*(8), 1474–1484.

Lloyd, J., and J. A. Taylor (1994), On the temperature dependence of soil respiration, *Funct. Ecol.*, *8*(3), 315–323.

Mendelssohn, I. A., and J. T. Morris (2000), Eco-physiological controls on the productivity of Spartina alterniflora Loisel, in *Concepts and Controversies in Tidal Marsh Ecology*, edited by M. P. Weinstein and D. A. Kreeger, pp. 59–81, Springer, Netherlands.

Millette, T. L., B. A. Argow, E. Marcano, C. Hayward, C. S. Hopkinson, and V. Valentine (2010), Salt marsh geomorphological analyses via integration of multitemporal multispectral remote sensing with LIDAR and GIS, *J. Coastal Res.*, *26*(5), 809–816.

Moffett, K. B., A. Wolf, J. A. Berry, and S. M. Gorelick (2010), Salt marsh-atmosphere exchange of energy, water vapor, and carbon dioxide: Effects of tidal flooding and biophysical controls, *Water Resour. Res.*, *46*, W10525, doi:10.1029/2009WR009041.

Moore, C. (1986), Frequency response corrections for eddy correlation systems, *Boundary Layer Meteorol.*, *37*(1–2), 17–35.

Morris, J. T., and B. Haskin (1990), A 5-yr record of aerial primary production and stand characteristics of Spartina alterniflora, *Ecology*, *71*(6), 2209–2217.

Morris, J. T., P. Sundareshwar, C. T. Nietch, B. Kjerfve, and D. cahoon (2002), Responses of coastal wetlands to rising sea level, *Ecology*, *83*(10), 2869–2877.

Morris, J. T., K. Sundberg, and C. S. Hokinson (2013), Salt marsh primary production and its responses to relative sea level and nutrients in estuaries at Plum Island, Massachusetts, and North Inlet, South Carolina, USA, *Oceanography*, *26*(3), 78–84.

Mudd, S. M., A. D'Alpaos, and J. T. Morris (2010), How does vegetation affect sedimentation on tidal marshes? Investigating particle capture and hydrodynamic controls on biologically mediated sedimentation, *J. Geophys. Res.*, *115*, F03029, doi:10.1029/2009JF001566.

Novick, K., J. Walker, W. Chan, A. Schmidt, C. Sobek, and J. Vose (2013), Eddy covariance measurements with a new fast-response, enclosed-path analyzer: Spectral characteristics and cross-system comparisons, *Agric. For. Meteorol.*, *181*, 17–32.

Nyman, J. A., R. J. Walters, R. D. Delaune, and W. H. Patrick Jr. (2006), Marsh vertical accretion via vegetative growth, *Estuarine Coastal Shelf Sci.*, *69*(3–4), 370–380.

Papale, D., et al. (2006), Towards a standardized processing of net ecosystem exchange measured with eddy covariance technique: Algorithms and uncertainty estimation, *Biogeosciences*, *3*(4), 571–583.

Rastetter, E., et al. (2010), Processing Arctic eddy-flux data using a simple carbon-exchange model embedded in the ensemble Kalman filter, *Ecol. Appl.*, *20*(5), 1285–1301.

Reichstein, M., et al. (2005), On the separation of net ecosystem exchange into assimilation and ecosystem respiration: Review and improved algorithm, *Global Change Biol.*, *11*(9), 1424–1439.

Rocha, A. V., and G. R. Shaver (2009), Advantages of a two band EVI calculated from solar and photosynthetically active radiation fluxes, *Agric. For. Meteorol.*, *149*(9), 1560–1563.

Schäfer, K. V. R., R. Tripathee, F. Artigas, T. H. Morin, and G. Bohrer (2014), Carbon dioxide fluxes of an urban tidal marsh in the Hudson-Raritan estuary, *J. Geophys. Res. Biogeosci.*, *119*, 2065–2081, doi:10.1002/2014JG002703.

Schedlbauer, J. L., S. F. Oberbauer, G. Starr, and K. L. Jimenez (2010), Seasonal differences in the CO_2 exchange of a short-hydroperiod Florida Everglades marsh, *Agric. For. Meteorol.*, *150*(7-8), 994–1006.

Shaver, G. R., L. E. Street, E. B. Rastetter, M. T. Van Wijk, and M. Williams (2007), Functional convergence in regulation of net CO_2 flux in heterogeneous tundra landscapes in Alaska and Sweden, *J. Ecol.*, *95*(4), 802–817.

Troxler, T. G., J. G. Barr, J. D. Fuentes, V. Engel, G. Anderson, C. Sanchez, D. Lagomasino, R. Price, and S. E. Davis (2015), Component-specific dynamics of riverine mangrove CO_2 efflux in the Florida Coastal Everglades, *Agric. For. Meteorol.*, *213*, 273–282.

Valiela, I., J. M. Teal, and N. Y. Persson (1976), Production and dynamics of experimentally enriched salt marsh vegetation: Belowground biomass1, *Limnol. Oceanogr.*, *21*(2), 245–252.

Valiela, I., J. M. Teal, and W. G. Deuser (1978), The nature of growth forms in the salt marsh grass Spartina alterniflora, *Am. Nat.*, *112*(985), 461–470.

Wilson, C. A., Z. J. Hughes, D. M. FitzGerald, C. S. Hopkinson, V. Valentine, and A. S. Kolker (2014), Saltmarsh pool and tidal creek morphodynamics: Dynamic equilibrium of northern latitude saltmarshes?, *Geomorphology*, *213*, 99–115.

Wilson, T., and T. Meyers (2007), Determining vegetation indices from solar and photosynthetically active radiation fluxes, *Agric. For. Meteorol.*, *144*(3–4), 160–179.

Wohlfahrt, G., S. Pilloni, L. Hörtnagl, and A. Hammerle (2010), Estimating carbon dioxide fluxes from temperate mountain grasslands using broad-band vegetation indices, *Biogeosciences*, *7*(2), 683–694.

Yan, Y., B. Zhao, J. Chen, H. Guo, Y. Gu, Q. Wu, and B. Li (2008), Closing the carbon budget of estuarine wetlands with tower-based measurements and MODIS time series, *Global Change Biol.*, *14*(10), 2469–2471.

Yan, Y.-E., H.-Q. Guo, Y. Gao, B. Zhao, J.-Q. Chen, B. Li, and J.-K. Chen (2010), Variations of net ecosystem CO_2 exchange in a tidal inundated wetland: Coupling MODIS and tower-based fluxes, *J. Geophys. Res.*, *115*, D15102, doi:10.1029/2009JD012838.